Applied Catalysis B: Environmental 87 (2009) 245–251

Contents lists available at ScienceDirect

Applied Catalysis B: Environmental

journal homepage: www.elsevier.com/locate/apcatb

Gold/hydroxyapatite catalysts
Synthesis, characterization and catalytic activity to CO oxidation

M.I. Domínguez *, F. Romero-Sarria, M.A. Centeno, J.A. Odriozola

Dpto. de Química Inorgánica e Instituto de Ciencia de Materiales de Sevilla, Centro Mixto Universidad de Sevilla-CSIC, Avda. Américo Vespucio 49, 41092 Sevilla, Spain

ARTICLE INFO

Article history:
Received 2 July 2008
Received in revised form 18 September 2008
Accepted 19 September 2008
Available online 27 September 2008

Keywords:
Gold
Hydroxyapatite
CO oxidation
Vacancies
Peroxides

ABSTRACT

This work reports the synthesis, characterization and catalytic activity for CO oxidation of gold catalysts supported on calcium hydroxyapatite. On both, the hydroxyapatite support and the gold-supported hydroxyapatite catalyst, the CO conversion shows a peak near 100% of conversion at room temperature. The generation of structural vacancies by interaction of CO with the solid provokes the formation of peroxide species in the presence of gaseous oxygen, which seems to be responsible of this high conversion of CO at room temperature. Moreover, the influence of the pre-treatment temperature on the activity has been observed and related with the elimination of carbonate species and the generation of structural defects in the apatite structure, which are able to modify the gold oxidation state.

1. Introduction

Supported gold nanoparticles have been demonstrated to be useful in many applications among them heterogeneous catalysis [1]. Since Haruta et al.'s work [2], CO oxidation on oxide-supported gold catalysts has been extensively studied, being the high activity at low temperatures the driving force for these studies [3–23].

Several mechanisms have been proposed for explaining this high catalytic activity in the oxidation of CO at low temperature when gold is dispersed in form of nanoparticles on metallic oxides.

The high catalytic activity of supported gold clusters has been associated to quantum size effects, particle morphology and size and gold oxidation state [4,9,10,17]. The existence of oxygen vacancies also influences the catalytic activity. Several explanations supported on experimental and theoretical data have been proposed for this effect [3,11,13,14,22], among them, negative charging of Au_8 clusters interacting with F-centre defects of MgO supports [11] or modification of gold dispersion and oxidation state on CeO_2 [22]. Further support for the role of vacancies on the catalytic activity is found when the effect of water on the catalytic activity for CO oxidation is studied [7,8,21,23].

It is generally accepted that reducible oxides such as α-Fe_2O_3, TiO_2 and lately CeO_2 [6,19,22,24–26] are active supports due to their capability to provide reactive oxygen and, hence, it might be assumed that oxygen vacancies play a role on the catalytic oxidation of CO on supported gold clusters. Hernández et al. [14], in a theoretical study, found that a high electron density on gold atoms placed at the Au/TiO_x interface facilitates oxygen activation.

Calcium hydroxyapatite (HAp) $Ca_{10}(PO_4)_6(OH)_2$ belongs to the crystallographic group of apatites, isomorphic compounds of general formula $Me_{10}(XO_4)_6Y_2$, where Me is a divalent cation, XO_4 an anionic trivalent group and Y a monovalent anion. These compounds crystallize in the hexagonal system (point group $P6_3/m$) and their structure can be described as a compact assemblage of Me ions and tetrahedral XO_4 groups delimiting two types of unconnected channels [27] (Fig. 1). The first one has a diameter of 2.5 Å and is delimited by four Me, denoted MeI. In the second type of channel there are six Me, named MeII, placed in two equilateral triangles at 1/4 and 3/4 and centred in a C_6-axis. This type of channel has a diameter of 3.5 Å, is oriented along the *c*-axis and hosts the Y anions, which balance the positive charge of the matrix and have great mobility [28]. The apatite structure is very flexible; all the elements can be exchanged if the charge balance is maintained. Moreover, these compounds present a high chemical and thermal stability and a weak and retrograde solubility. These properties make them useful in several applications like biomaterials, optics, radioactive and industrial wastes immobilization or catalysis. Although this material has been scarcely used for supporting gold, the reported data show the suitability of this support for preparing gold catalysts active in the oxidation of CO [29,30].

* Corresponding author. Tel.: +34 954489543; fax: +34 954460665.
E-mail address: mleal@icmse.csic.es (M.I. Domínguez).

0926-3373/$ – see front matter © 2008 Elsevier B.V. All rights reserved.
doi:10.1016/j.apcatb.2008.09.016

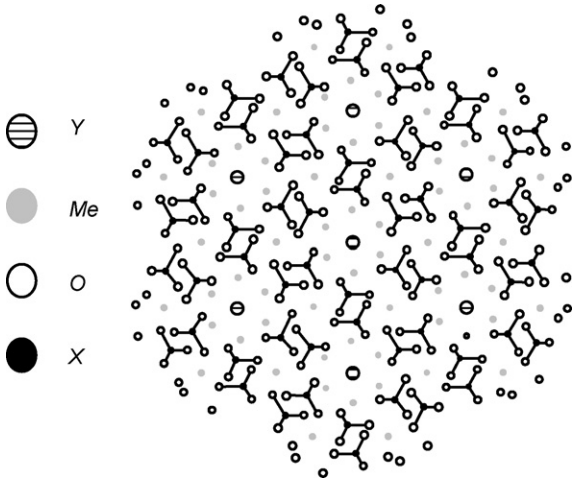

Fig. 1. Projection of apatite structure over the plane 001.

The complex crystallochemistry of apatites may result in non-reducible supports in which the presence of defects can be tailored by substitution in either cationic or anionic sites [31,32]. In this work, we use the method proposed by Wang et al. [33] to produce well-defined hydroxyapatite nanorods at low synthesis temperatures by chemical precipitation from an aqueous solution containing an organic modifier, which acts controlling the size and morphology of the hydroxyapatite crystals. The election of the method was done to obtain a material with high specific surface area. This synthesis procedure results in the formation of rod-like carbonated hydroxyapatites that upon heating generate vacancies at the anionic sites. In the prepared systems, the influence of the pre-treatment on the catalytic activity in the oxidation of CO has been observed, allowing the study of the effect of the presence of vacancies in the support for non-reducible materials.

2. Experimental

The reactants used to synthesize the catalysts were phosphoric acid 85% (Panreac), calcium nitrate tetrahydrate (Merck), ammonia 30% (Panreac), sodium citrate dihydrate (Panreac) and hydrogen tetrachloroaurate (Alfa).

Aqueous solutions of phosphoric acid 0.6 M and calcium nitrate 1 M (ratio Ca/P 1.67, characteristic of calcium hydroxyapatite) were mixed into a flask that was kept at 40 °C in a water bath. Then, an aqueous solution containing sodium citrate dihydrate (5% by weight of the HAp theoretically produced) was added to this solution under stirring and the pH of the reaction solution was adjusted to 10 by the addition of an ammonium solution (30%). The resultant solution was reacted for 8 h at 40 °C. After that, the reaction solution was transferred into a Teflon-lined autoclave and heated at 100 °C for 8 h. Finally, the resultant powders were washed with deionised water until pH 7 and dried at 100 °C overnight. The prepared support was named HAp.

A deposition-precipitation process was used to prepare the gold-hydroxyapatite catalyst, denoted as Au/HAp. The required amount of $HAuCl_4.3H_2O$ for synthesizing 0.5% by weight gold catalysts was dissolved in distilled water and the pH adjusted to 9 with NaOH 0.1 M. The solution was heated at 65 °C and then the support was added, keeping the mixture under vigorous stirring at 65 °C for 1 h [34]. After this time, the catalyst was separated by filtration, washed with deionised water to remove chloride and Na^+, and dried overnight at 100 °C.

CO oxidation catalytic tests were carried out in a conventional continuous flow U-shaped glass reactor working at atmospheric pressure. Eighty milligrams of the catalyst, 100–200 mm particle size, were placed between two plugs of glass wool; the reaction temperature was monitored by a thermocouple in contact with the catalyst bed. The reaction products were analyzed by mass spectrometry, using a Balzers Thermostar benchtop mass spectrometer controlled by the software Balzers Quadstar 422 with capabilities for quantitative analysis. Light-off curves for CO oxidation were obtained from RT to 300 °C at a heating rate of 5 °C min^{-1}. A mixture containing 3.4% CO (Air Liquide, 99.997% pure, <3 ppm H_2O) and 21% O_2 (Air Liquide, 99.999% pure, <3 ppm H_2O) in He (Air Liquide, 99.999% pure, <3 ppm H_2O) at a total flow rate of 42 mL min^{-1} was used for all the catalytic tests. Empty reactor (without catalyst) shows no activity under such conditions. The catalysts were pre-activated *in situ* during 1 h at 300 or 400 °C flowing a mixture containing 21% O_2 in He at a total flow rate of 30 ml min^{-1} and then stabilized at room temperature before the light-off curve started.

Gold content of the obtained catalysts was measured by X-ray fluorescence (XRF), employing a PANalytical AXIOS sequential spectrophotometer with a rhodium tube as source of radiation. XRF measurements were performed onto pressed pellets (sample including 6 wt.% of wax).

X-ray diffraction (XRD) analysis was carried out on a Siemens diffractometer D500. Diffraction patterns were recorder with Cu Kα radiation (40 mA, 40 kV) over a 2θ range of 10–70° and a position-sensitive detector using a step size of 0.05° and a step time of 1 s.

The textural properties were studied by N_2 adsorption–desorption measurements at liquid nitrogen temperature. The experiences were performed in a Micromerits ASAP 2010 equipment. Before analysis, the samples were degassed for 2 h at 150 °C in vacuum.

Transmission electron microscopy (TEM) observations were carried out in a Philips CM200 microscope operating at 200 kV. The samples were dispersed in ethanol by sonication and dropped on a copper grid coated with a carbon film.

DRIFTS spectra were obtained in a Thermo Nicolet Nexus infrared spectrometer with a KBr optic and a MCT/B detector working at liquid nitrogen temperature. An environmental DRIFTS chamber (Spectra-Tech 0030-101) equipped with ZnSe windows, allowing *in situ* treatments up to 600 °C and 1 atm., was coupled to the spectrometer. The sample was placed inside the chamber without packing or dilution. The spectra of pure samples, heated until 300 °C in different atmospheres, were obtained by co-adding 64 scans at 4 cm^{-1} resolution. The spectrum obtained for an aluminium mirror was used as background.

3. Results and discussion

The chemical composition of the support and gold-supported catalyst was obtained by XRF. The measured calcium-to-phosphorous atomic ratio is 1.93 which is higher than the one corresponding to ideal hydroxyapatite [$Ca_{10}(PO_4)_6(OH)_2$], Ca/P = 1.67, suggesting that carbonate groups replace structural phosphate groups. Carbonate ions may substitute the apatite structure [32,33,35–37], they may be located either into the channels, replacing OH^- groups (A-type substitution) or in the framework, substituting phosphate groups (B-type substitution). Carbonated apatites with Ca-to-P ratios as high as 2.07 has been described for biological and mineral apatite materials [35,36]. Our support might be formulated as $Ca_{9.45}(PO_4)_{4.90}(CO_3)_{1.10}(OH)_2$, a stoichiometry close to that found by Lafon et al. [32] in their synthesis procedure. The measured gold content of the Au/HAp catalyst is 0.48% (w/w) very close to the targeted value of 0.5%.

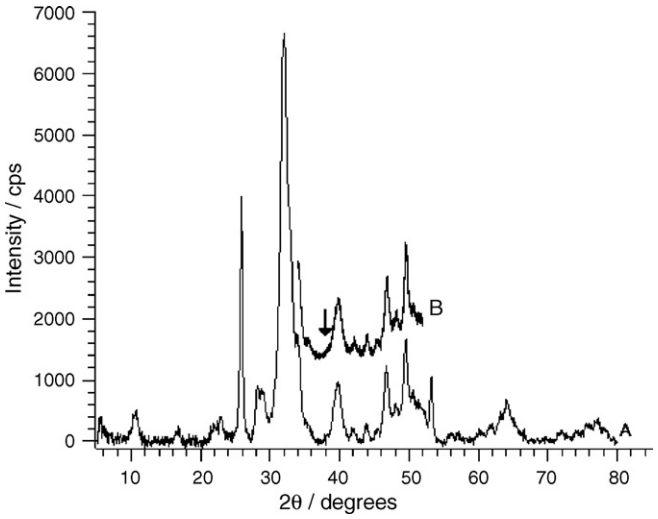

Fig. 2. (A) XRD diagram of the hydroxyapatite support; (B) XRD diagram of the Au-supported catalysts in the region relevant for the diffraction of the cubic phase of gold. An arrow marks the position of the gold diffraction line with the highest intensity.

Hydroxyapatite is the only crystalline phase formed in HAp as stated by XRD measurements, Fig. 2. The XRD diagram of the gold catalyst does not show diffraction lines corresponding to gold, the main gold diffraction line is marked with an arrow in the figure. The rest of the diffraction lines, omitted for the sake of simplicity, are indistinguishable from those of the HAp diagram. The low loading and/or a very small particle size may account for this fact.

Both the support and the catalysts present N_2 type IV adsorption–desorption isotherms, characteristic of solids consisting of particles having nearly cylindrical channels or made by aggregates or agglomerates of spheroidal particles. A H1 hysteresis loop indicates pore of uniform size and shape, Fig. 3A.

The textural properties of the studied samples are compiled in Table 1. The BET surface area, pore volume and average pore size do not change significantly on depositing gold. The hysteresis loop and the pore size distribution clearly indicate the existence of interparticle porosity (Fig. 3).

TEM micrographs of the HAp support show relatively uniform particles of ca. 50 nm of length, with a rod-like shape with a length-to-diameter ratio between 10 and 15. Upon gold deposition the size and shape of the hydroxyapatite crystals do not change, as it should be expected for the textural data. Gold particles can hardly be seen by TEM, the number of gold particles is smaller than expected for the deposited amount of gold (0.5% by weight), Fig. 4. A catalyst constituted by very small gold crystals (diameter below 5 nm) distributed homogeneously over HAp together with few colloidal gold agglomerated particles, having sizes between 5 and 15 nm, is suggested from the TEM and SEM data. By SEM gold particles cannot be seen (results not shown), discarding the gold agglomeration in bigger particles. This is consistent with the very recent data of Phonthammachai et al. [30] for the synthesis of gold-supported hydroxyapatite catalysts and recent studies of gold nanocrystals loaded on phosphate containing supports. These studies suggest that phosphate groups prevent the agglomeration of Au crystals and increase the activity for the oxidation of CO [38,39].

The Au-supported catalyst shows excellent activity for the oxidation of CO even at room temperature, Fig. 5. Despite the unusual shape of the light-off curve, the CO conversion is higher than 50% in all the temperature range studied achieving 100% conversion at 25–30 °C and above 200 °C. The support shows very

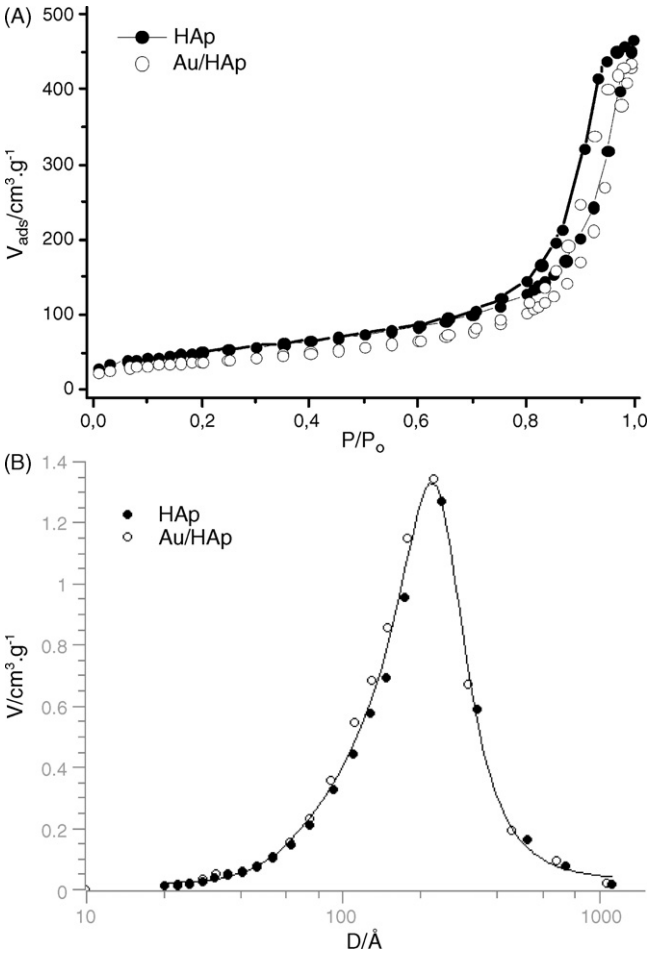

Fig. 3. (A) N_2 adsorption–desorption isotherms of the support and the gold catalysts; (B) pore size distribution.

low activity for CO oxidation, ca. 10% at 300 °C. This unusual shape for the light-off curves has been reported by other authors [20,25,40,41] and has been related by Simakov et al. [42] to the coexistence of several gold species that are active in different temperature ranges. These authors associated the activity at low temperatures with the presence of $Au_n^{\delta+}$ or Au_n^0 clusters (gold species with the diameter less than 1 nm and $n \leq 8$) and the activity at high temperatures with the existence of Au^0 gold nanoparticles (particles with a diameter between 1.5 and 20 nm) [52]. The modification of gold oxidation state, particle size and dispersion with the reduction temperature would alter the activity for CO oxidation, explaining the influence of the activation temperature in the light-off curves shown in Fig. 5. The pre-treatment temperature would modify the nature of the gold active centres and hence the catalytic activity. However, on going from 300 to 400 °C in the catalyst pre-treatment does not alter the catalyst textural properties or gold particle size as previously reported [30] but, nevertheless, affects the chemical composition of the hydroxyapatite support. Fig. 6 presents the MS data obtained for the gold catalyst during the pre-treatment process in

Table 1
Textural properties of the prepared solids calcined at 300 °C.

Sample	S_{BET} ($m^2\ g^{-1}$)	V_p ($cm^3\ g^{-1}$)	d_p (Å)
HAp	129	0.52	162.8
Au/HAp	140	0.59	168.4

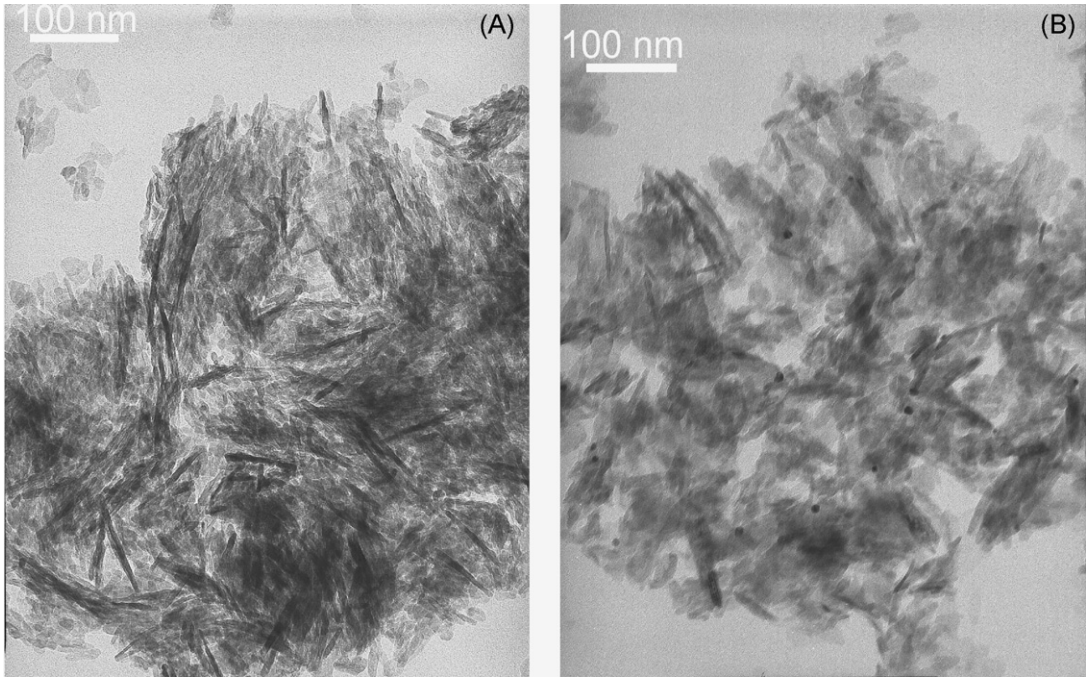

Fig. 4. TEM micrographs of HAp (A) and Au/HAp (B) materials.

a 21% O_2 in He flow. The CO_2 signal is composed by three peaks at 311, 335 and 383 °C, indicating the decomposition of several types of carbonates, with different stability. These carbonate ions are transformed in a neutral species (CO_2), remaining the negative charges in the structure. The hydroxyapatite support is not easily reduced, neither PO_4^{3-} nor Ca^{2+} are reduced at room temperature, however, the gold species are easily reducible. Thus, the elimination of carbonate groups would affect the oxidation state of gold nanoparticles that, taking into consideration the activity data, Fig. 4, are not fully reduced, since the low temperature activity for the oxidation of CO is associated to the presence of partially reduced gold species [42]. This indicates that the differences in activity detected for the catalyst when pre-treated at 400 °C have to be related with the elimination of carbonate species and the generation of structural defects in the apatite structure, which modify the gold oxidation state.

In addition to this, it is worth mentioning the appearance even in the support of a first conversion peak at room temperature that reaches values near 100% of conversion. This high CO conversion for the support alone, even thought the very short temperature range, has to be associated to the chemical nature of the support as previously suggested for gold catalysts supported on phosphates of phosphate modified titania [30,38,39], although no explanations has been proposed for this fact. In order to explain this phenomenon, we study the oxidation of CO over the Au/HAp catalyst by *in situ* DRIFTS. Once the catalyst is activated at the desired pre-treatment temperature, the DRIFTS cell is allowed to cool down and infrared spectra were recorded under two different flows: (a) 21% O_2/He and (b) 3.4% CO/21% O_2/He.

Fig. 7 shows DRIFTS spectra recorded in both conditions for the Au/HAp catalyst. It is necessary to emphasize that the band

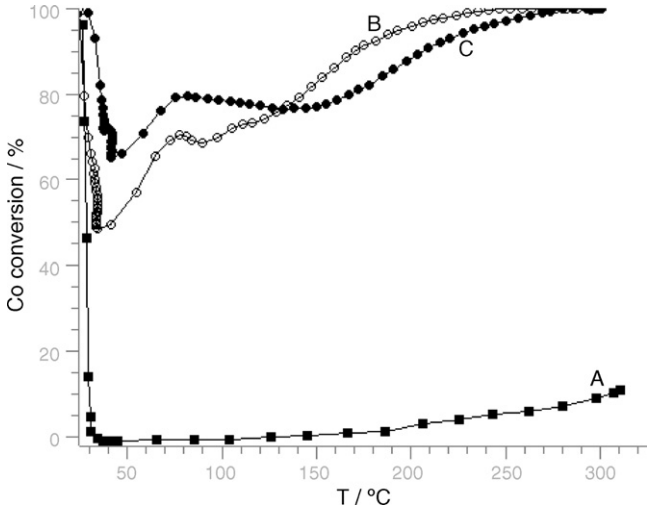

Fig. 5. CO oxidation light-off curves: (A) hydroxyapatite support pretreated at 400 °C; (B) Au-supported hydroxyapatite catalyst pretreated at 300 °C and (C) Au-supported hydroxyapatite catalyst pretreated at 400 °C.

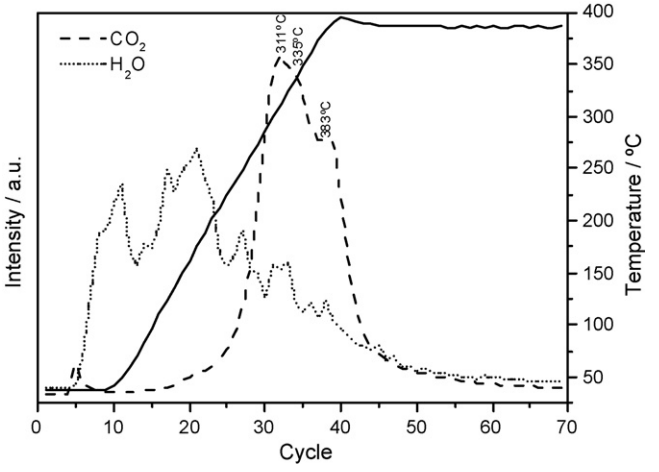

Fig. 6. MS signal obtained during the pre-treatment process (21% O_2/He flow) for the gold-supported hydroxyapatite catalyst.

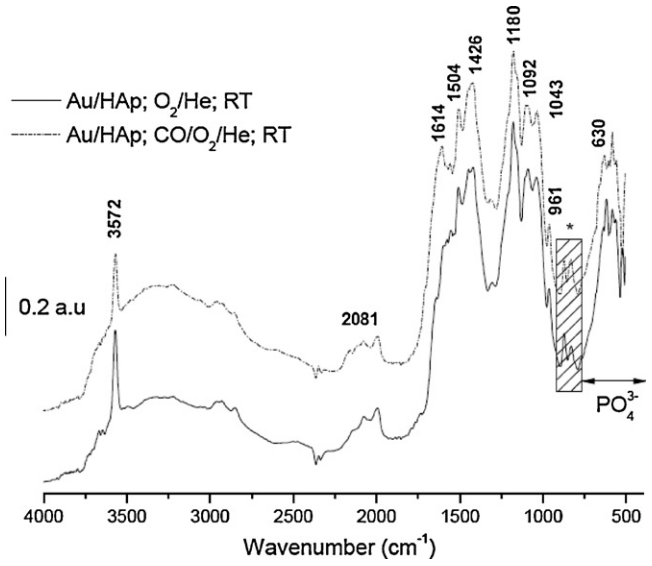

Fig. 7. DRIFT spectra obtained at room temperature of the gold-supported hydroxyapatite catalyst under 21% O_2/He flow and 3.4% CO/21% O_2/He flow.

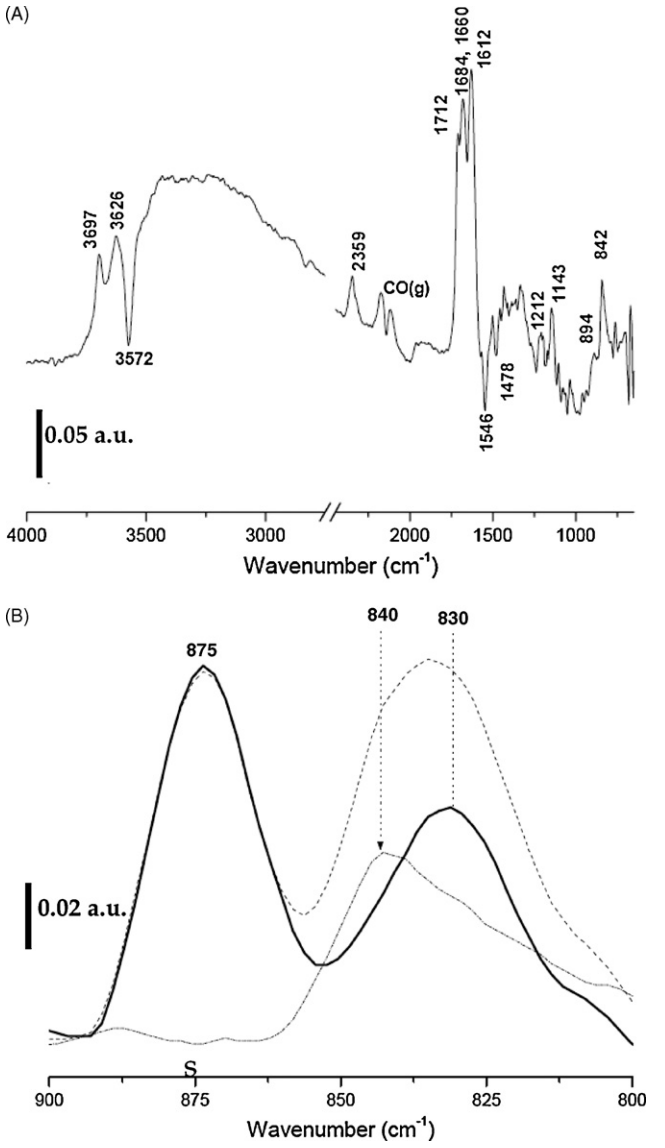

Fig. 8. (A) Difference DRIFT spectrum obtained by subtracting to the DRIFT spectrum of the Au/HAp catalyst submitted to a 3.4% CO/21% O_2/He flow at room temperature the DRIFT spectrum of the same catalyst obtained under a 21% O_2/He flow at room temperature; (B) DRIFT spectra in the 900–800 cm^{-1} region for the Au/HAp catalyst submitted to: 21% O_2/He flow at room temperature (continuous line), 3.4% CO/21% O_2/He flow (dotted line) and substraction spectrum (denoted as "S" in the figure).

corresponding to CO adsorbed on gold species is not clearly observed due to the presence of CO in gas phase into the DRIFT cell. Since the intensity of this band (CO gas) depends on the quantity of gas into the cell and it is a function of the conversion, the reference spectrum to subtract the gas phase is not constant in intensity. Therefore, the bands corresponding to the adsorbed species are masked, being very difficult the total (or correct) elimination of the gas phase contribution. The bands at 3572 and 630 cm^{-1} are attributed to the stretching and librational modes, of OH groups in the hydroxyapatite structure, respectively [43]. Moreover, bands at 1092, 1043 and 961 cm^{-1} are due to asymmetric and symmetric stretching vibrations of phosphate groups [44]. The bending mode of PO_4^{3-} appears at ca. 600 cm^{-1} (647, 620 and 584 cm^{-1}). Harmonic overtones or combination bands of phosphate groups appear around 2000 cm^{-1}.

On the other hand, the A-type carbonate species in apatite structures are characterised by IR absorption bands at 1545, 1450 cm^{-1} (asymmetric and symmetric stretching vibration) and a singlet at 880 cm^{-1}, while the type B carbonates show bands at 1455, 1410, 875 cm^{-1}. The A-type carbonate may be placed in two different positions, which are denoted by A1 and A2. The bands typical of these species appear in the same spectral region, but at frequencies slightly modified: the A2 species appears at higher frequencies than the A1 one [32,33,36,37]. In the presented spectra, the intense, broad and not well-defined group of bands appearing in the 1300–1600 cm^{-1} region includes the typical bands of carbonate species and those associated to the bending vibration of water (1614 cm^{-1}). In this way, IR results confirm the presence of carbonates; suggested by XRF analysis, and explain the carbon dioxide evolution shown in Fig. 6.

HPO_4^{2-} may also be present in the hydroxyapatite as impurities [43]. According to Petrov et al. [45], the band at 1180 (with a shoulder at 1150 cm^{-1}) could be attributed to the P–O stretching mode of these species. Although pure hydroxyapatite shows a combination band at 1154 cm^{-1}, the presence of anhydrous dicalcium phosphate in the sample cannot be discarded. The P–O(H) stretching vibration of dicalcium phosphates (865–875 cm^{-1}) [44] has also been detected. The broad band in the 3500–2500 cm^{-1} region together with the band at 1614 cm^{-1} confirms the presence of adsorbed water on the surface of the catalyst.

In order to clearly evidence the modifications produced under the reaction flow, a difference spectrum between the two spectra shown in Fig. 7 has been obtained (Fig. 8A). The two branches of the rotational spectrum of gas phase CO with a minimum at 2143 cm^{-1} is observed; a single band at 2359 cm^{-1} is ascribed to CO_2 adsorbed on acid sites of the surface. The presence of adsorbed CO_2 confirms the results obtained in a conventional reactor (Fig. 5): the CO oxidation proceeds at room temperature in this catalyst.

In addition, a group of intense bands appears in the 1800–1500 cm^{-1} region. The second derivative study indicates the presence of bands at 1712, 1684, 1660 and 1612 cm^{-1}. According to the attribution of Petrov et al. [45] and the thermal stability studies (results not shown), it is possible to assign the two firsts bands to dicalcium phosphate dihydrate (DCPD) and those at 1660 and 1612 cm^{-1} to bending mode of water molecules adsorbed on the surface [46]. The stretching of O–H groups of water molecules

adsorbed on the surface appears at 3697 and 3626 cm^{-1}. The apparition of bands at 1212 and 1143 cm^{-1} also confirms the presence of DCPD.

The negative bands of low intensity at 1546 and 1478 cm^{-1} indicate the perturbation of carbonate species by interaction with the flow of reaction ($CO/O_2/He$).

At this point, it is interesting to focus the discussion on the 900–800 cm^{-1} region (marked with an asterisk in Fig. 7 and enlarged in Fig. 8B). This region is specially complicated in this catalytic system, since carbonate species (A and B types) and dicalcium phosphates (anhydrous and dihydrated) present vibrational modes active in the infrared in this zone of the spectrum. Moreover, bands corresponding to the π mode of carbonate groups adsorbed on the surface of metallic oxides have been found at ca. 835 cm^{-1} [22]. Considering these factors, this region has to be studied more in detail and taking into account the changes produced by the presence of CO in the flow. The bands at 875 and 830 cm^{-1} evidence the presence of both dicalcium phosphates and carbonate species for the catalyst submitted to O_2/He flow. On adding CO to the reaction flow the band at 875 cm^{-1} remains unaltered suggesting that $CaHPO_4$ species are not affected while the band at 830 cm^{-1} shifts to slightly higher frequencies and increases its intensity. The difference spectrum, Fig. 8B, clearly states that the generation of a new species characterised by a vibrational mode at 840 cm^{-1} is responsible for the modification of the DRIFT spectrum in the presence of CO. This band cannot be ascribed to DCPD since its P–O(H) vibrational mode appears at higher frequencies, around 900 cm^{-1} [45]. In addition to this, a different evolution with temperature is observed for this vibrational mode and that peaking at 1712 cm^{-1}, unequivocally ascribed to DCDP. Following a similar reasoning, this band cannot be ascribed to carbonate species since the generation of bands in the 1550–1400 cm^{-1} region of the spectrum is not observed.

An alternative explanation to the formation of DCDP or carbonate groups is the generation, in the presence of oxygen, of peroxide species that present vibrational modes in the 800–900 cm^{-1} region of the spectrum [47]. Carrettin et al. [48] attributed the increasing of the activity of a Fe-doped TiO_2 to the vacancies formation during the doping, and established that these defects activate the oxygen, favouring the CO oxidation reaction. They also detected the formation of superoxide species in presence of oxygen. Moreover, Rossignol et al. [49] observed peroxide species by FTIR spectroscopy after oxygen adsorption on pre-reduced ceria catalysts. These facts point out the relationship existing between vacancies and oxidative species formation by reaction with oxygen. In the case of hydroxyapatite structure, the same effect was observed in presence of oxygen [50,51].

In our case, the CO oxidation at room temperature has been verified both by observing adsorbed CO_2 by DRIFTS and gas phase evolution using mass spectrometry. This carbon dioxide evolution correlates with the occurrence of the infrared band (840 cm^{-1}) ascribed to the formation of peroxide species on the catalyst surface. Therefore, this oxidative species should be responsible for the CO oxidation catalytic activity at room temperature for both the hydroxyapatite support and the gold-supported hydroxyapatite catalyst.

When the flow containing CO and oxygen starts to pass through the catalyst, the CO interaction with the hydroxyl groups (evidenced by the vanishing of the band at 3572 cm^{-1}) provokes an alteration of the electrostatic equilibrium into the channel. This decreasing of the number of OH groups probably occurs through the formation of HPO_4^{2-} species according to the following stoichiometric scheme: $Ca_{10-z}(PO_4)_{6-z}(HPO_4)_z(OH)_{2-z}$, where $0 \leq z \leq 1$ [50]. The vacancies created previously are now able to react with the oxygen present in the flow and the peroxide species becomes visible to the IR. These species may be responsible of the CO oxidation to CO_2. The quantity of HPO_4^{2-} groups that may be included in the hydroxyapatite structure is limited ($0 \leq z \leq 1$). Therefore, once the equilibrium is raised, the CO_2 production stops. This fact explains why only one peak of conversion is observed at room temperature in a flow of CO and oxygen and the presence of DCPD in the FTIR spectra.

4. Conclusions

High surface hydroxyapatites obtained by a low temperature synthesis method are adequate to be used as gold supports. The prepared gold/hydroxyapatite catalyst shows good activity in the catalytic CO oxidation. The influence of the pre-treatment temperature in the catalytic activity has been observed and related with the generation of structural vacancies by the elimination of carbonates, which modify the gold oxidation state. A peak of CO conversion at room temperature that reaches values near 100% has been detected. By means of DRIFTS *in situ*, this fact has been associated with structural changes and formation of vacancies where oxygen can be activated to produce peroxide species, responsible of this room temperature CO oxidation.

Acknowledgements

Financial support for this work has been obtained from Junta de Andalucía (Plan Andaluz de Investigación, grupo TEP106) and Ministerio de Educación y Ciencia, MEC (MAT2006-12386-C05). F. Romero-Sarria thanks the MEC for her Ramón y Cajal contract.

References

[1] G.C. Bond, C. Louis, D.T. Thompson, Catalysis by Gold, Imperial College Press, London, 2006.
[2] M. Haruta, N. Yamada, T. Kobayashi, S. Iijima, J. Catal. 115 (1989) 301–309.
[3] M. Haruta, Catal. Today 36 (1997) 153–166.
[4] M. Valden, X. Lai, D.W. Goodman, Science 281 (1998) 1647–1650.
[5] G.C. Bond, D.T. Thompson, Catal. Rev. Sci. Eng. 41 (1999) 319–388.
[6] A.C. Gluhoi, M.A.P. Dekkers, B.E. Nieuwenhuys, J. Catal. 219 (2003) 197–205.
[7] C.K. Costello, J.H. Yang, H.Y. Law, Y. Wang, J.N. Lin, L.D. Marks, M.C. Kung, H.H. Kung, Appl. Catal. A 243 (2003) 15–24.
[8] H.H. Kung, M.C. Kung, C.K. Costello, J. Catal. 216 (2003) 425–432.
[9] J. Guzman, S. Carrettin, A. Corma, J. Am. Chem. Soc. 127 (2005) 3286–3287.
[10] L. Fu, N.Q. Wu, J.H. Yang, F. Qu, D.L. Johnson, M.C. Kung, H.H. Kung, V.P. Dravid, J. Phys. Chem. B 109 (2005) 3704–3706.
[11] B. Yoon, H. Hakkinen, U. Landman, A.S. Worz, J.M. Antonietti, S. Abbet, K. Judai, U. Heiz, Science 307 (2005) 403–407.
[12] M.A. Centeno, C. Portales, I. Carrizosa, J.A. Odriozola, Catal. Lett. 102 (2005) 289–297.
[13] I.N. Remediakis, N. López, J.K. Nørskov, Angew. Chem., Int. Ed. 44 (2005) 1824–1826.
[14] N.C. Hernández, J.F. Sanz, J.A. Rodríguez, J. Am. Chem. Soc. 128 (2006) 15600–15601.
[15] R. Burch, Phys. Chem. Chem. Phys. 8 (2006) 5483–5500.
[16] M.A. Centeno, K. Hadjiivanov, T. Venkov, H. Klimev, J.A. Odriozola, J. Mol. Catal. A 252 (2006) 142–149.
[17] G.J. Hutchings, M.S. Hall, A.F. Carley, P. Landon, B.E. Solsona, C.J. Kiely, A. Herzing, M. Makkee, J.A. Moulijn, A. Overweg, J.C. Fierro-Gonzalez, J. Guzman, B.C. Gates, J. Catal. 242 (2006) 71–81.
[18] T. Venkov, H. Klimev, M.A. Centeno, J.A. Odriozola, K. Hadjiivanov, Catal. Commun. 7 (2006) 308–313.
[19] S.K. Hashmi, G.J. Hutchings, Angew. Chem. Int. Ed. 45 (2006) 7896–7936.
[20] J.G. Carriazo, L.M. Martínez, J.A. Odriozola, S. Moreno, R. Molina, M.A. Centeno, Appl. Catal. B 72 (2007) 157–165.
[21] M. Okumura, M. Haruta, Y. Kitagawa, K. Yamaguchi, Gold Bull. 40 (2007) 40–44.
[22] F. Romero-Sarria, L.M. Martínez, M.A. Centeno, J.A. Odriozola, J. Phys. Chem. C 111 (2007) 14469–14475.
[23] F. Romero-Sarria, A. Penkova, L.M. Martínez T, M.A. Centeno, K. Hadjiivanov, J.A. Odriozola, Appl. Catal. B 84 (2008) 119–124.
[24] M.A. Centeno, M. Paulis, M. Montes, J.A. Odriozola, Appl. Catal. A 234 (2002) 65–78.
[25] L.M. Martínez, D.M. Frías, M.A. Centeno, A. Paúl, M. Montes, J.A. Odriozola, Chem. Eng. J. 136 (2008) 390–397.
[26] M.I. Domínguez, M. Sánchez, M.A. Centeno, M. Montes, J.A. Odriozola, Appl. Catal. A 302 (2006) 96–103.

[27] J.C. Elliot, Structure and Chemistry of the Apatites and other Calcium Orthophosphates, Elsevier Science, 1994.
[28] Z. Boukha, M. Kacimi, M.F.R. Pereira, J.L. Faria, J.L. Figueiredo, M. Ziyad, Appl. Catal. A 317 (2007) 299–309.
[29] A. Venugopal, M.S. Scurrell, Appl. Catal. A 245 (2003) 137–147.
[30] N. Phonthammachai, Z. Ziyi, G. Jun, H.Y. Fan, T.J. White, Gold Bull. 41 (2008) 42–50.
[31] M.I. Domínguez, J. Carpena, D. Borschnek, M.A. Centeno, J.A. Odriozola, J. Rose, J. Hazard. Mater. 150 (2008) 99–108.
[32] J.P. Lafon, E. Champion, D. Bernache-Assollant, J. Eur. Ceram. Soc. 28 (2008) 139–147.
[33] A. Wang, H. Yin, D. Liu, H. Wu, M. Ren, T. Jiang, X. Cheng, Y. Xu, Mater. Lett. 61 (2007) 2084–2088.
[34] Y.F. Han, N. Phonthammachai, K. Ramesh, Z. Zhong, T. White, Environ. Sci. Technol. 42 (2008) 908–912.
[35] A.M. Abed, K. Fakhouri, Chem. Geol. 131 (1996) 1–13.
[36] B. Wopenka, J.D. Pasteris, Mater. Sci. Eng. C 25 (2005) 131–143.
[37] M.E. Fleet, X. Liu, J. Solid State Chem. 177 (2004) 3174–3182.
[38] Z. Ma, S. Brown, S.H. Overbury, S. Dai, Appl. Catal. A 327 (2007) 226–237.
[39] W. Yan, S. Brown, Z. Pan, S.M. Mahurin, S.H. Overbury, S. Dai, Angew. Chem. Int. Ed. 45 (2006) 3614–3618.
[40] A. Gluhoi, Fundamental studies focused on understanding of gold catalysis, Thesis, Leiden University, 2005.
[41] J.L. Margitfalvi, A. Fási, M. Hegedus, F. Lónyi, S. Gobölös, N. Bogdanchikova, Catal. Today 72 (2002) 157–169.
[42] A. Simakov, I. Tuzovskaya, A. Pestryakov, N. Bogdanchikova, V. Gurin, M. Avalos, M.H. Farías, Appl. Catal. A 331 (2007) 121–128.
[43] M. Markovic, B.O. Fowler, M.S. Tung, J. Res. Natl. Ins. Stand. Technol. 109 (2004) 553–568.
[44] S. Koutsopoulos, J. Biomed. Mater. Res. 62 (2002) 600–612.
[45] I. Petrov, B. Soptrajanov, N. Fuson, J.R. Lawson, Spectrochim. Acta 23 (1967) 2637–2646.
[46] L. Tortet, G.R. Gavarri, G. Nihoul, A.J. Dianoux, J. Solid State Chem. 132 (1997) 6–16.
[47] T. Itoh, T. Maeda, A. Kasuya, Faraday Discuss. 132 (2006) 95–109.
[48] S. Carrettin, Y. Hao, V. Aguilar-Guerrero, B.C. Gates, S. Trasobares, J.J. Calvino, A. Corma, Chem. Eur. J. 13 (2007) 7771–7779.
[49] S. Rossignol, F. Gérard, D. Duprez, J. Mater. Chem. 9 (1999) 1615–1620.
[50] Y. Matsumura, H. Kanai, J.B. Moffat, J. Mol. Catal. A 135 (1998) 317–320.
[51] Y. Matsumura, H. Kanai, J.B. Moffat, J. Mol. Catal. A 115 (1997) L229–L232.
[52] I. Tuzovskaya, N. Bogdanchikova, A. Simakov, V. Gurin, A. Pestryakov, M. Avalos, M.H. Farías, Chem. Phys. 338 (2007) 23–32.